JOURNAL OF Materials CHEMISTRY

Semiporous MoS_2 obtained by the decomposition of thiomolybdate precursors

Astrid Leist,[a] Sandra Stauf,[a] Sandra Löken,[a] E. Wolfgang Finckh,[a] Silke Lüdtke,[a] Klaus K. Unger,[a] Wolfgang Assenmacher,[b] Werner Mader[b] and Wolfgang Tremel[a]*

[a]*Institut für Anorganische Chemie und Analytische Chemie, Johannes Gutenberg-Universität, Mainz, Becher Weg 24, D55099 Mainz, Germany*

[b]*Institut für Anorganische Chemie, Universität Bonn, D53117 Bonn, Germany*

The decomposition of three different ammonium thiomolybdates $(NH_4)_2MoS_4 \cdot xH_2O$, $(NH_4)_2Mo_2S_{12} \cdot xH_2O$, and $(NH_4)_2Mo_3S_{13} \cdot xH_2O$ ($x = 1$–2) have been studied by TG–DSC under argon. While all three thiomolybdates decompose at around 673 K to yield nearly X-ray amorphous MoS_2, the precursor $(NH_4)_2Mo_3S_{13} \cdot xH_2O$ does so in a manner distinct from the other two precursors displaying a sharp exothermic peak in the DSC trace. We suggest that the unusual thermal behaviour of $(NH_4)_2Mo_3S_{13} \cdot xH_2O$ might arise from a topochemical relation between the molecular cluster and 2*H*-MoS_2 as proposed previously. The porosity of the X-ray amorphous MoS_2 obtained from the decomposition under vacuum of $(NH_4)_2Mo_3S_{13} \cdot xH_2O$ is unusually large and the material displays interesting sorption behaviour towards small organic molecules. This X-ray amorphous semiporous modification of MoS_2 has been characterized in detail by powder X-ray diffraction, high resolution electron microscopy and from its extended X-ray absorption fine structure. An unusual feature of this material is the presence of bent, open-ended lamellae of MoS_2, contrasting fullerene-like MoS_2 which forms closed shells.

The structure and properties of binary molybdenum sulfides are of special interest because of their enormous potential as lubricants[1] and as hydrodesulfurization catalysts.[2] Crystalline MoS_2 has a lamellar structure which is what makes it an effective lubricant. The introduction of curvature in the structure of small MoS_2 crystallites allows the formation of nested fullerene-like structures, resembling carbon nanotubes and onions.[3] These nested fullerene-like structures have no dangling bonds making them even more effective as lubricants than bulk crystalline 2*H*-MoS_2.[4] Small particles of MoS_2 are also of interest because they display quantum size effects.[5] To our knowledge, no attempt has been made to prepare MoS_2 in semiporous or mesoporous modifications. While intercalation in crystalline MoS_2 is possible through the process of exfoliation and restacking,[6] an MoS_2 derived material that shows sorption properties without pretreatment through exfoliation has not been reported so far.

The decomposition of thiomolybdate precursors to yield, eventually, crystalline 2*H*-MoS_2 has been studied extensively by Müller and co-workers.[7–10] Of particular interest is their study of the decomposition of $(NH_4)_2Mo_3S_{13} \cdot xH_2O$[10] which yielded 2*H*-$MoS_2$ after extended heating. These authors identified the topochemical relationship between the trinuclear cluster in the thiomolybdate and the disposition of Mo and S in the stable thermodynamic product, namely, 2*H*-MoS_2. In this contribution we provide further evidence for the importance of this topochemical relation by comparing the decomposition behaviour of three different thiomolybdates. The main thrust of this contribution is, however, our finding that performing the decomposition of $(NH_4)_2Mo_3S_{13} \cdot xH_2O$ under conditions of dynamic vacuum yields a nearly X-ray amorphous material with large surface area and large pore sizes. In comparision, the decomposition of $(NH_4)_2Mo_3S_{13} \cdot xH_2O$ under the conditions of ref. 10 are reported to yield materials with much smaller surface areas.

The decomposition of $(NH_4)_2Mo_3S_{13} \cdot xH_2O$ has been followed by powder X-ray diffraction. One of the porous products has been characterised by high resolution electron microscopy and from an analysis of its extended X-ray absorption fine structure. We also report preliminary attempts to use the X-ray amorphous semiporous modification as a host to sorb small organic molecules.

Experimental

The three thiomolybdates used in this study were synthesised using procedures from the literature: $(NH_4)_2MoS_4 \cdot xH_2O$,[11] $(NH_4)_2Mo_2S_{12} \cdot xH_2O$,[12] and $(NH_4)_2Mo_3S_{13} \cdot xH_2O$.[13] Differential thermal analysis–differential scanning calorimetry (DTA–DSC) was carried out on 0.035 g of each of the samples in quartz boats under flowing argon using a Netzsch STA429 instrument. The thermal protocol included a ramp from room temperature to 873 K at a rate of 5 K min^{-1}, a soak at 873 K for 60 min followed by cooling to room temperature at 5 K min^{-1}. The cycle was then repeated without the soak. For powder X-ray diffraction (XRD) studies, $(NH_4)_2Mo_3S_{13} \cdot xH_2O$ samples were heated in sealed vitreous silica tubes at different temperatures for 24 h periods after which the tubes were quenched in water. The XRD patterns were recorded in θ–2θ transmission geometry using a Siemens D5000 diffractometer and monochromatized Cu-Kα_1 radiation. UV–VIS spectra of the decomposition products were recorded on a Varian Cary 5G spectrometer in the diffuse reflectance mode. $BaSO_4$ was used as an optical diluent. FTIR spectra were recorded with the samples pressed into pellets with KBr. The BJH pore sizes and BET surface areas of the decomposition products were determined using N_2 as the probe molecule on a Micromeritics instrument. Scanning electron microscopy (SEM) of the decomposition products was performed on a Zeiss microscope and high-resolution transmission electron microscopy (HRTEM) at the University of Bonn.

X-Ray absorption spectra at the Mo K edge were acquired at the EXAFS3 station on the DCI beamline at LURE, Orsay, France with well ground samples being held between adhesive tape. The storage ring is operated at 1.85 GeV with 250 mA current at the time of the data acquisition. The X-rays were monochromatized using a silicon 331 channel-cut monochromator, detuned to supress higher harmonics. The incident energy was scanned between 19.9 and 21.0 keV in steps of

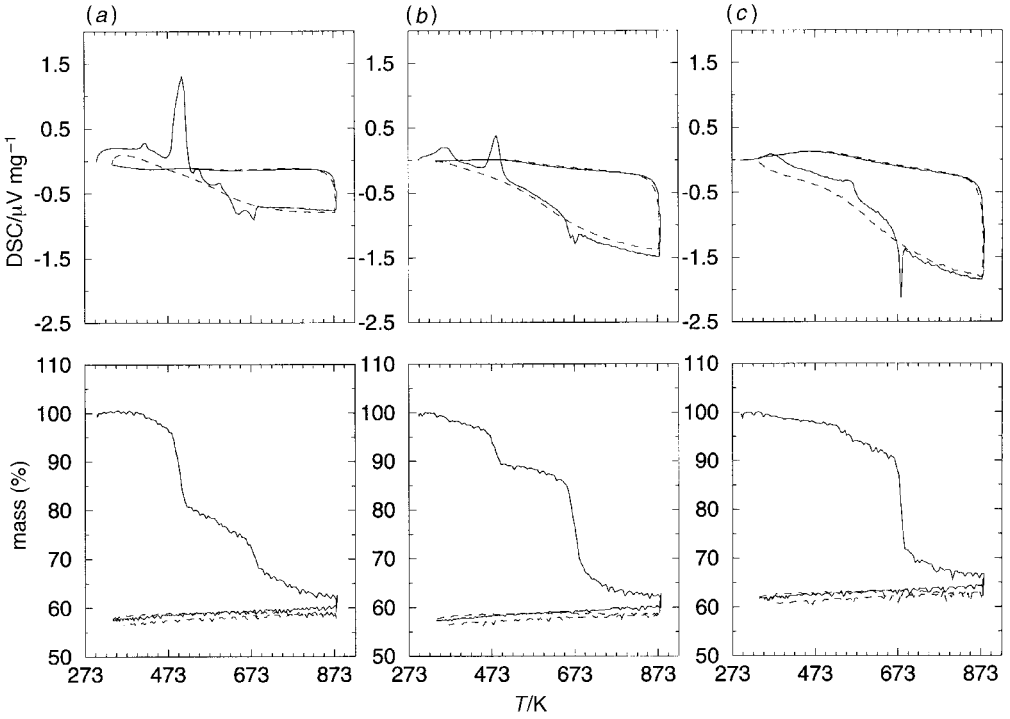

Fig. 1 DSC and DTA traces for the three thiomolybdates: (*a*) $(NH_4)_2MoS_4 \cdot xH_2O$, (*b*) $(NH_4)_2Mo_2S_{12} \cdot {}_xH_2O$, (*c*) $(NH_4)_2Mo_3S_{13} \cdot xH_2O$

2 eV, with a scan time of 2 s per step. Three scans were averaged before data reduction.

Results and Discussion

Fig. 1 shows the DSC–DTA traces of the three thiomolybdate precursors. The first cycle is depicted using continuous lines and the second using dashed lines. Both $(NH_4)_2MoS_4 \cdot xH_2O$ and $(NH_4)_2Mo_2S_{12} \cdot xH_2O$ display small endotherms in the DSC traces corresponding to the loss of water below 473 K. At temperatures between 473 and 673 K, all three compounds show endotherms in the DSC traces and a corresponding mass loss in the DTA. This corresponds to the loss of sulfur and ammonia. In the vicinity of 673 K the samples show exotherms and the stabilization of the mass that commences at this temperature suggests that MoS_2 is formed in a small temperature window above 673 K. What is interesting from Fig. 1 is the observation of a sharp exotherm near 673 K in the DSC trace of $(NH_4)_2Mo_3S_{13} \cdot xH_2O$. Sharp exotherms are not observed in the DSC traces of the other two compounds. This lends credence to the picture of a topochemical transformation of the trinuclear $[Mo_3S_{13}]^{2-}$ cluster to hexagonal MoS_2 with loss of S^{2-}. From calculations of the mass loss observed from the DTA traces, all three thiomolybdates decompose to give products with nominal compositions near MoS_2.

To follow the crystallization, powder XRD patterns were recorded on the decomposition products obtained from $(NH_4)_2Mo_3S_{13} \cdot xH_2O$ after heating at specific temperatures in sealed vitreous silica tubes. Fig. 2 shows the XRD patterns thus obtained. The temperatures at which the heating was carried out are indicated. While the XRD pattern of the starting material is retained after heating until 573 K, the pattern obtained after 673 K begins to show the principal 002 reflection of MoS_2 corresponding to interlamellar spacings between 6 and 7 Å. Further heating results in the main peak becoming sharper and other peaks of 2*H*-MoS_2 appearing. Even after heating at 1073 K, the pattern does not correspond to perfectly crystalline 2*H*-MoS_2. We have simulated faulted MoS_2 using the procedures incorporated in the DIFFAX computer program.[14] The results of visual comparison of experimental (1073 K) and simulated XRD patterns are consistent with up to 20% random fcc-type stacking along the *c* axis interrupting the otherwise hcp-type stacking of 2*H*-MoS_2. Additionally, we have used arbitrary thermal broadening of the stacking vectors in the modelling procedure corresponding to poor registry between adjacent lamellae. The simulated diffraction patterns were convoluted with instrumental profile parameters which were in turn obtained from Rietveld

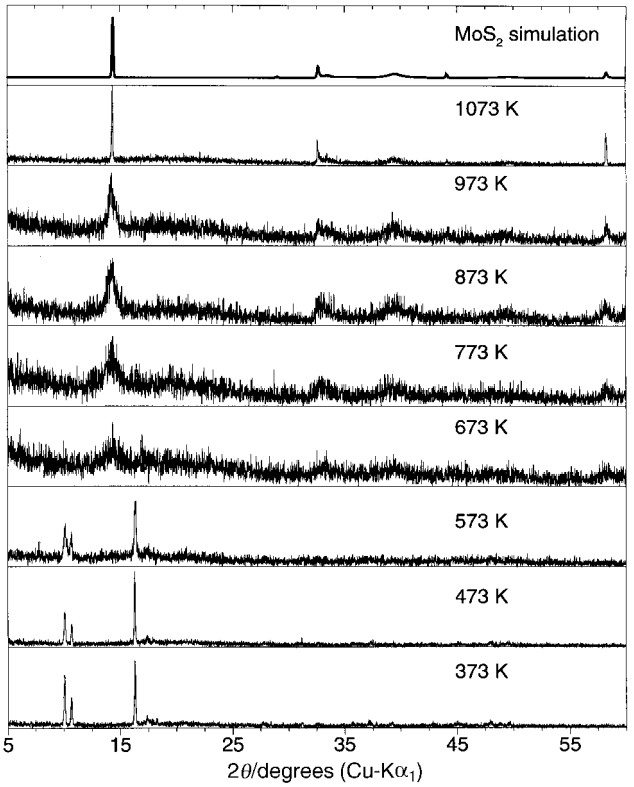

Fig. 2 Powder X-ray diffraction patterns observed following the heating of $(NH_4)_2Mo_3S_{13} \cdot xH_2O$ for 24 h in sealed evacuated vitreous silica tubes at the temperatures indicated. A simulated diffraction pattern is also shown (simulation details in text).

refinement on standard compounds using the computer program FULLPROF.[15]

Since the diffraction patterns obtained after heating $(NH_4)_2Mo_3S_{13}\cdot xH_2O$ at intermediate temperatures (673–873 K) do not yield much information, the more local structural probes of electron microscopy and extended X-ray absorption fine structures have been employed on a sample of X-ray amorphous MoS_2 prepared by heating the thiomolybdate under static vacuum (in a sealed tube) at 673 K for 48 h followed by heating at 473 K under dynamic (rotary) vacuum for 24 h. Fig. 3(a) shows an SEM picture of the product. The needle like morphology of the material is preserved from the morphology of the precursor. In Fig. 3(b) a HRTEM image of the same material is shown. Despite the material being amorphous to X-rays, layered microcrystallites of MoS_2 with an interlayer spacing (half the *c* parameter) between 6 and 7 Å are clearly visible. What is interesting is that portions of the micrographs show curved regions similar in disposition to what is observed in carbon soots or microcrystalline graphite.[16] In fact, the nature of the material whose micrograph is shown in Fig. 3(b) is related to the nested fullerene-like structures of Tenne and co-workers[3] in much the same way that carbon soot is related to the carbon onions observed by Ugarte.[17] As found in carbon soot, the lamellae of MoS_2 seen here are bent but there are no closed structures observed. This bending of lamellae can result in turbostratic disorder and hence the sawtooth structure of the *hk*0 peaks observed in the region of $2\theta = 32^\circ$ in the diffraction patterns of material obtained by heating above 773 K. However, turbostratic disorder and hence sawtooth *hk*0 line shapes can also result by shearing the layers with respect to each other rather than bending them as observed here. This is the classical model of Wildervanck and Jellinek[18] for the crystallinity of MoS_2. The observation of bent but not nested lamellae of MoS_2 is, to our knowledge, novel.

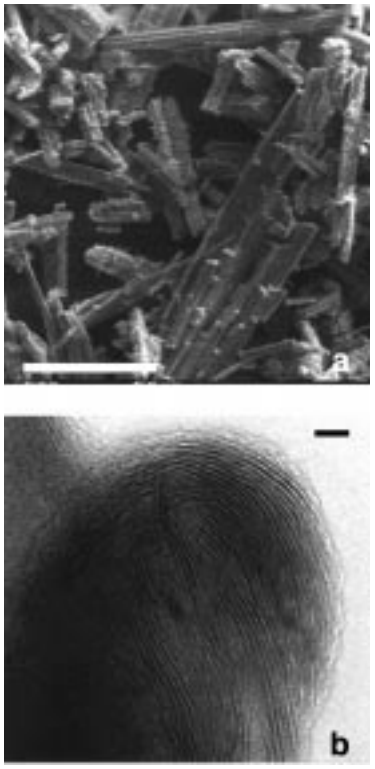

Fig. 3 (a) SEM image of the material obtained after decomposition of $(NH_4)_2Mo_3S_{13}\cdot xH_2O$ at 673 K in a sealed tube followed by 473 K in dynamic vacuum. The scale bar corresponds to 50 μm. (b) HRTEM image of the same material showing a bent lamellar structure. The scale bar corresponds to 2 nm.

While the lamellae observed in the HRTEM images suggest a close relation to the structure of crystalline MoS_2, this is further strengthened by the modelling of EXAFS oscillations. The upper panel of Fig. 4 shows the Fourier transform and fit of the EXAFS. The program of Michalowicz[19] was used for this purpose. The phase and amplitude functions were extracted using crystalline 2*H*-MoS_2 as a standard. In the lower panel of Fig. 4, we show the atomic pair distribution function around Mo as obtained from the fit. We fix for each Mo atom, six S nearest neighbors and obtain a distance of 2.42(3) Å. The second coordination shell was then well refined with 4.7(6) Mo neighbors at a distance of 3.15(5) Å. For comparison, the distances in 2*H*-MoS_2 are six S at 2.43 Å and six Mo at 3.16 Å. The Debye–Waller factor was detemined to be $\sigma = 0.02(1)$ and the correlation coefficient between Mo occupancy and σ was *ca.* 0.6 which is acceptable.

The diffuse reflectance UV–VIS spectrum of the amorphous MoS_2 is displayed in Fig. 5 along with the UV–VIS spectrum

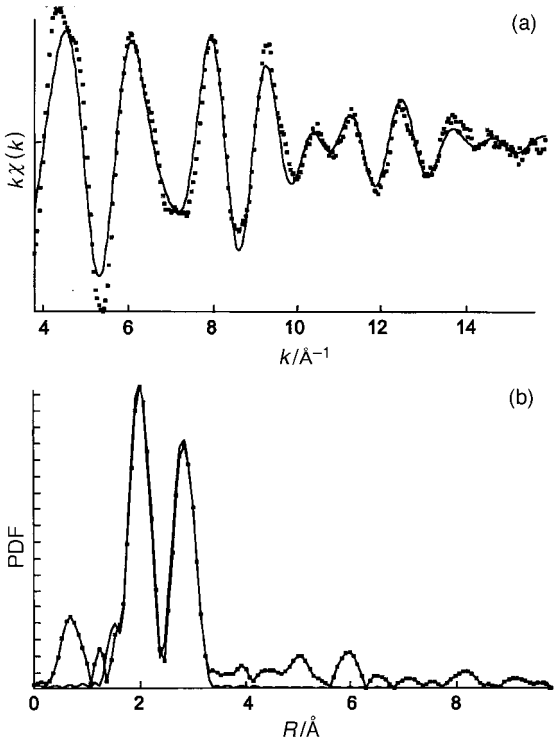

Fig. 4 (a) Fourier transform and fit of the EXAFS signal. (b) Atomic pair distribution function around Mo consistent with the Fourier transform. (■ data, — fit)

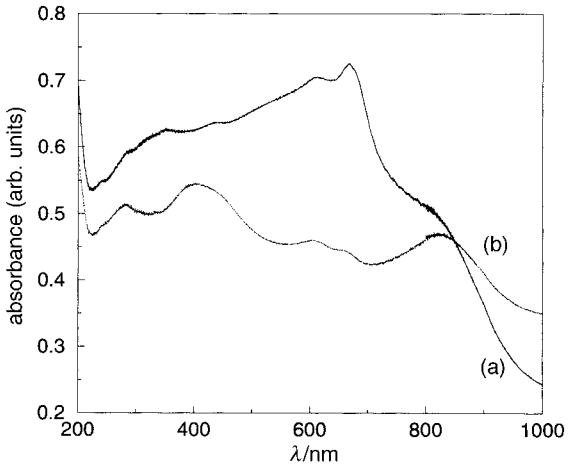

Fig. 5 Diffuse reflectance UV–VIS absorption spectra of 2*H*-MoS_2 (a) and amorphous MoS_2 (b)

Table 1 Sorption behaviour of the products obtained from the decomposition of $(NH_4)_2Mo_3S_{13}\cdot xH_2O$ at 473 K for different durations[a]

heat treatment, t/h[b]	BET surface area/$m^2\ g^{-1}$	BJH pore diameter/Å adsorption/desorption	BJH pore volume/mg ml^{-1} adsorption/desorption
24	60.5	104.1/83.7	0.146/0.144
30	51.3	130.6/149.7	0.178/0.169
36	64.3	110.0/86.7	0.171/0.169
42	49.3	127.3/128.3	0.173/0.168
48	57.4	97.5/80.7	0.138/0.134
54	64.4	71.0/58.2	0.109/0.109

[a]The BET surface areas of crystalline and restacked MoS_2 are 5.8 and 10 $m^2\ g^{-1}$ respectively.[20] [b]At 473 K under dynamic vacuum. The material was pretreated by heating under static vacuum (sealed tubes) at 673 K for 48 h.

of polycrystalline 2*H*-MoS_2 for comparison. The spectra are plotted as absorption *vs.* wavelength rather than the more usual representation of reflectance *vs.* wavenumber or energy in order to facilitate comparison with ref. 5. The absorption edge near 700 nm in the spectrum of 2*H*-MoS_2 results from the direct transition between the Γ and K points in the Brillouin zone.[5] The peak like features just below this edge correspond to excitonic transitions, and at still lower energies, to transitions whose exact nature is unknown. The spectrum of the amorphous MoS_2 on the other hand, shows a strong similarity in form if not in energy to the spectrum of quantum confined 4.5 nm MoS_2 particles in solution.[5] The overall red-shift in the present case using the 4.5 nm particles as a reference is of the order of 300 nm. This is undoubtedly due to the larger sizes of the MoS_2 particles in the X-ray amorphous MoS_2. We note that the comparison of diffuse reflectance spectra with absorption spectra is fraught with difficulties particularly in the scaling of energy.

The nature of the HRTEM image encouraged us to investigate the sorption behaviour of the X-ray amorphous MoS_2 as obtained here in order to see whether the curvature of the lamellae results in pores and cavities that might serve as hosts for the sorption of small guest molecules. In Table 1, we present the results of such investigations using dinitrogen as the probe molecule. The data is shown for the measurements on samples of $(NH_4)_2Mo_3S_{13}\cdot xH_2O$ that were initially heated in a static vacuum (sealed tubes) for 48 h at 673 K followed by heating in a dynamic vacuum at 473 K for the times indicated. From all aspects, the surface area, the pore diameter and the pore volume, it is clear that thermal decomposition of $(NH_4)_2Mo_3S_{13}\cdot xH_2O$ results in materials with exceptional properties. For comparison, we have taken from the literature[20] data on the BET surface areas of crystalline and restacked (after exfoliation) MoS_2. The sizes of the pores are in the range of what are referred to as mesoporous materials. Similar sorption behaviour is observed in the products obtained by the decomposition of $(NH_4)_2Mo_2S_{12}\cdot xH_2O$. Our investigations suggest that both the heat treatment and the presence of vacuum are necessary for porous materials to be obtained. We speculate that the driving out of volatile materials from the precursor might, in addition to the ability of the MoS_2 lamellae to form curved surfaces, assist in the formation of morphologies with large pores. In that sense, there is some exfoliation involved in the present case as well. Indeed FTIR spectra of the decomposition products indicate the continued presence of the ammonium ions as seen from ν_{N-H} in the range 3500–3300 cm^{-1}.

We have made some preliminary efforts to fill the pores with small molecules such as ferrocene and polymers such as polyethylene oxide. This was achieved by the vigorous stirring of the X-ray amorphous MoS_2 in solutions of the respective molecules, followed by extensive washing of the material with the same solvent. FTIR spectra suggest that the organic guest is retained in the host structure. The process must however be distinguished from intercalation since we have no evidence for insertion of small molecules between the MoS_2 lamellae. In a crystalline material, the process of intercalation is traditionally established from the expansion of lattice parameters. This becomes difficult in an X-ray amorphous material.

In ref. 7, thiomolybdates are dispersed and decomposed on high-surface area alumina in order to obtain catalysts. The material presented here avoids the problem of requiring a support since it is intrinsically of high porosity and surface area.

We thank Professor Guy Ouvrard of the IMN, Nantes for help in acquiring the EXAFS spectra and Volkmar Derstroff for the UV–VIS spectra. This work has been supported by the Fonds der Chemischen Industrie and the Deutsche Forschungsgemeinschaft. We thank Heraeus Quarzschmelze Hanau (Dr. Höfer) for a generous gift of silica tubes.

References

1 I. L. Singer, in *Fundamentals of Friction: Macroscopic and Microscopic Processes,* ed. I. L. Singer and H. M. Pollock, Kluwer, Dordrecht, 1992.
2 D. Delmon, *Bull. Soc. Chim. Belg.,* 1995, **104**, 173.
3 Y. Feldman, E. Wasserman, D. J. Srolovitz and R. Tenne, *Science,* 1995, **267**, 222; M. Hershfinkel, L. A. Gheber, V. Volterra, J. L. Hutchison, L. Margulis and R. Tenne, *J. Am. Chem. Soc.,* 1994, **116**, 1914.
4 L. Rapoport, Y. Bilik, Y. Feldman, M. Homyonfer, S. R. Cohen and R. Tenne, *Nature* (*London*), 1997, **387**, 791.
5 J. P. Wilcoxon and G. A. Samara, *Phys. Rev. B.,* 1995, **51**, 7299.
6 W. M. R. Divigalpitiya, R. F. Frindt and S. R. Morrison, *Science,* 1990, **246**, 369; E. Ruiz-Hitzky, R. Jiminez, B. Casal, V. Manriques, A. Santa Ana and G. Gonzalez, *Adv. Mater.,* 1993, 738; E. Ruiz-Hitzky, *Adv. Mater.,* 1993, 334; H. Tagaya, T. Hashimoto, M. Karasu, T. Izumi and K. Chiba, *Chem. Lett.,* 1992, 213.
7 A. Müller, E. Diemann, A. Branding, F. W. Baumann, M. Breysse and M. Vrinat, *Appl. Catal.,* 1990, **62**, L13.
8 T. P. Prasad, E. Diemann and A. Müller, *J. Inorg. Nucl. Chem.,* 1973, **35**, 1895.
9 A. Müller and E. Diemann, *Chimia,* 1985, **39**, 312.
10 E. Diemann, A. Müller and P. R. Aymonino, *Z. Anorg. Allg. Chem.,* 1981, **479**, 191.
11 G. Krüss, *Justus Liebigs Ann. Chem.,* 1884, **225**, 6.
12 A. Müller, R. G. Bhattacharya and B. Pfefferkorn, *Chem. Ber.,* 1979, **112**, 778.
13 A. Müller, S. Sarkar, R. G. Bhattacharya, S. Pohl and M. Dartmann, *Angew. Chem., Int. Ed. Engl.,* 1978, **17**, 535.
14 M. M. J. Treacy, M. W. Deem and J. M. Newsam, Computer code DIFFAX v.1.801, 1990; *Proc. R. Soc. London A,* 1991, **433**, 499; *Ultramicroscopy,* 1993, **52**, 512.
15 J. Rodriguez-Carvajal, in *Proc. Satellite Meeting on Powder Diffraction of the XV Congress of the IUCr.,* Toulouse, France, 1990.
16 A. Oberlin, in *Chemistry and Physics of Carbon,* ed. P. A. Thrower, Marcel Dekker, New York 1988, pp. 1–143.
17 D. Ugarte, *Nature* (*London*), 1992, **359**, 707.
18 J. C. Wildervanck and F. Jellinek, *Z. Anorg. Allg. Chem.,* 1964, **328**, 309.
19 A. Michalowicz, *Logiciels pour la Chimie*, Société Française de Chimie, Paris, 1991, p. 102.
20 R. Bissessur, J. Heising, W. Hirpo and M. Kanatzidis, *Chem. Mater.,* 1996, **8**, 318.

Paper 7/05501C; *Received* 29*th July*, 1997